

Predicting Surface Roughness of Microcellular Foam Injection Parts molded by PC/N₂ System

Zhenyu XU¹, Chengzhi Ling², Chong Fan², Lihua Qin³, Kerong Wang¹ and Guanghong HU^{2*}

¹Mechanical & Electrical Engineering College, Jinhua Polytechnic, No.888 Haitang West Street, Jinhua, 321007, Zhejiang, China

²Institute of Forming Technology & Equipment, Shanghai Jiaotong University, No.1954, Huashan Road, Shanghai 200030, PR China

³Nanjing Zhonghezhiheng Information Technology Co., Ltd. No. 69 Feitian Road, Nanjing, 211113, Jiangsu, China

Article Info

*Corresponding author:

Guanghong HU

Institute of Forming Technology & Equipment
Shanghai Jiaotong University, No.1954
Huashan Road, Shanghai 200030
PR China
E-mail: hguangh@sju.edu.cn

Received: July 17, 2017

Accepted: July 25, 2017

Published: July 31, 2017

Citation: Xu Z, Ling C, Fan C, Qin L, Wang K, Hu G. Predicting Surface Roughness of Microcellular Foam Injection Parts molded by PC/N₂ System. *Madridge J Nanotechnol Nanosci.* 2017; 2(1): 65-72.
doi: 10.18689/mjnn-1000112

Copyright: © 2017 The Author(s). This work is licensed under a Creative Commons Attribution 4.0 International License, which permits unrestricted use, distribution, and reproduction in any medium, provided the original work is properly cited.

Published by Madridge Publishers

Abstract

Surface defects impose bottlenecks on industrial applications of microcellular foam injection molding. This study investigated the process starting from bubble nucleation and ending with surface defect formation. Results confirmed that surface bubbles trapped between injection parts and mold surfaces were the main cause of surface defects. Surface roughness values were first obtained with an accurate numerical surface roughness model. The surface roughness values calculated by numerical methods were compared with experimental results. The compared values were approximately equal, with a difference of 2.39 μm . Hence the mathematical analysis method adopted in this paper can accurately reflect actual processing conditions. Orthogonal methods were also applied to calculate the effect of process parameter variance on surface roughness.

Keywords: Bubble nucleation; Surface roughness; Surface-bubbles; Process parameters.

Introduction

Microcellular foam injection molding was first proposed by Prof. Nam Suh in the 1980s to save material in plastics processing. This process use supercritical fluids (SCF) as blowing agents without notably compromising the mechanical properties [1, 2]. Microcellular foam injection molding can be divided into four stages: (1) gas solution; (2) bubble nucleation; (3) bubble growth; (4) solidification. Compared with traditional foam injection molding, microcellular foam molding offers advantage in both physical part properties and processing stage. Microcellular foam injection parts contain bubble-population densities of $10^9 \sim 10^{12}$ cells/cm³ and bubble size of 1~100 μm , in addition to having excellent mechanical properties, dimensional stability, thermal stability and dielectric properties. Microcellular foam injection molding also has many advantages during processing: It reduces injection and packing pressure as well as processing cycle time [3, 4]. Because of the noteworthy prospects of saving energy and resources, microcellular foam injection molding has become an essential part of lightweight industrial applications.

Surface quality of microcellular foam injection parts has been the pivotal barrier limiting its industrial application, especially for exterior parts. Such surface quality defects include swirl marks, silver streaks, surface blistering and post-blow. Traditional surface finishing processes, such as grinding, polishing, and lapping, were difficult to eliminate these defects. Figure 1 illustrates the four main categories of surface defects caused by microcellular foam injection.

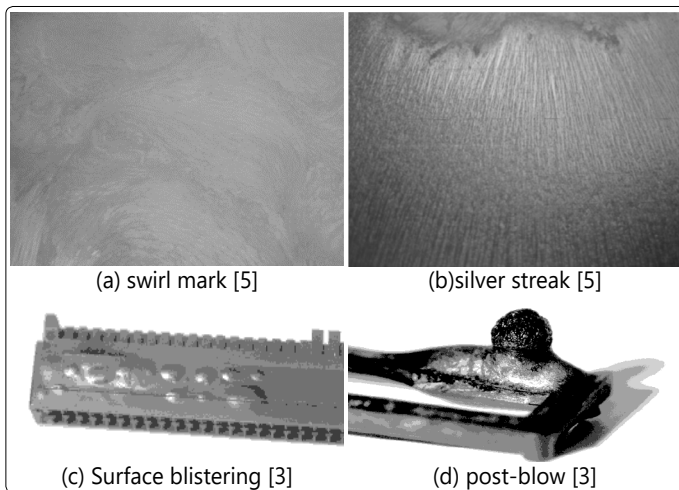


Figure 1. Surface defects of parts fabricated through microcellular foam injection

Cha and Yoon et al. indicated that swirl marks were caused by gas that was trapped on the mold surface when the polymer/gas solution began to solidify [6]. The bursting surface bubbles formed surface grooves, then the grooves combined and formed swirl marks. Michael and Cramer reported that silver streaks were engendered by macroscopic gas bubbles sheared against the cavity wall during the filling phase [7]. Surface blistering was assumed to be caused by macroscopic bubbles that did not burst (usually formed in the thin wall portions), and post-blow was assumed to be caused by high temperature at the hot spot [3]. All these surface defects have been reported to be caused by bubbles emerging onto surfaces after nucleation and then stretching to burst or scattering into tiny bubbles under shear stress between melt and mold surface. Morphological transformation of bubbles on part surfaces is the key factor affecting surface quality. Because of the positive correlation between surface roughness and surface defects, this study considers that surface roughness can be used as a quantitative indicator of surface defects, and the study assumed that the maximum surface roughness is formed when surface bubbles expand to their largest sizes and burst.

This article presents an accurate mathematical model of a surface roughness formation mechanism. This model was established and implemented in a simulation scheme with a PC/N₂ system. First, nucleation density and critical bubble size were simulated in MATLAB according to a modified microcellular foam nucleation theory. Subsequently, the injection molding process filling time and melt flow front temperature of a flat part were calculated in MOLDFLOW by using the former bubble data as a boundary condition. The final bubble size on the part surface was calculated by solving ordinary differential equations with a modified bubble growth theory. Finally, the final bubbles size on the part surface were converted into surface roughness values by a surface roughness mathematical model, and the roughness value of surface reference point approximated the experimentally observed value with an error of less than 3 μm. In addition, a series of orthogonal experiments were performed to demonstrate the effects of five processing parameters

affecting surface roughness (melt temperature, mold temperature, SCF content, melt pressure, injection time). Studies of bubble burst mechanisms on part surfaces are investigated in the next section.

Theories

Nucleation Theory

Classical nucleation theory was established by Gibbs in the twentieth century. It pointed out that nucleation was due to changes in external conditions that place the system into a thermodynamically unstable situation. When a bubble radius exceeds the critical radius of nuclear R*, the cell core can continue to expand steadily, eventually producing a bubble. In microcellular foam injection molding, the main reason for nucleation is the pressure drop from microcellular process pressure to flow front pressure. Microcellular foam nucleation processing can be described as homogeneous nucleation. On the basis of the classical microcellular foam nucleation theory established by Colton and Suh [8], some improvements have been made in the nucleation theory [3, 9, 10]. For the microcellular case, the modified Gibbs free energy of a single bubble can be characterized as follows [3].

$$\Delta_{mm}G = 4\pi R^2\gamma - \frac{n_g^n}{N} R_c T \ln \frac{n_g^n + n_g^*}{X_g^{sat}} + \frac{n_g^*}{N} R_c T \ln \frac{n_g^* / (n_g^n + n_g^*)}{1 - n_g^n} + \frac{1 - n_g^n - n_g^*}{N} R_c T \ln \frac{1}{1 - n_g^n} \quad (1)$$

where γ is the surface tension at the interface of the melt and the gas, n_gⁿ is mole of gas inside the bubbles in each mole of solution, n_g^{*} is mole of gas in the polymer in each mole of solution, n_gⁿ and n_g^{*} are the total moles of gas in each mole of solution, X_g^{sat} is the mole fraction of gas under saturation pressure, R_c is the ideal gas constant, N is the number of bubbles in each mole of solution, T is the absolute temperature (in K); this assumes the gas follows the ideal gas law.

At the critical point, the bubble system achieves a state of dynamic equilibrium in which the pressure inside the bubble P_g is the same as the initial saturation pressure P_{sat} and P_g = P_o + γ/R, where P_o is the melt pressure outside the bubble. Hence,

$$R^* = \frac{2\gamma}{P_{sat} - P_o} \quad (2)$$

If the pressure release rate is considered to be approximately constant, the quantity of nucleation per unit volume can be expressed as the integral of the nucleation rate per unit N₀ times the pressure, resulting in

$$N = \int_0^{t_g} N_0 dt = \int_{P_{sat}}^{P_g} \frac{N_0}{dP/dt} dP \quad (3)$$

The nucleation rate formula can be expressed as

$$N_0 = c_0 f_0 \exp\left(\frac{-\Delta G_{mm}}{KT}\right) \quad (4)$$

where c_0 is the number of gas molecules per volume, f_0 is the frequency value of homogeneous nucleation, and K is the Boltzmann constant. Using the pure polymer interface tension γ to calculate the nucleation rate and the initial nucleation radius in microcellular foam would be inappropriate. The interface tension after modified can be expressed as [11, 12]

$$\gamma_{mix} = \gamma_{polymer} \left(\frac{\rho_{mix}}{\rho_{polymer}} \right)^4 (1 - \omega_{gas})^4 \quad (5)$$

where $\gamma_{polymer}$ is the surface tension of pure polymer, ρ_i is the Moore density of i , and ω_{gas} is the weight fraction of gas. The nucleation rate can be obtained by solving equations 1, 3, 4.

Bubble Growth Theory

The unit cell model established by Amon and Denson [13] describes bubble growth in microcellular foam. Figure 2 shows the schematic of the unit cell model.

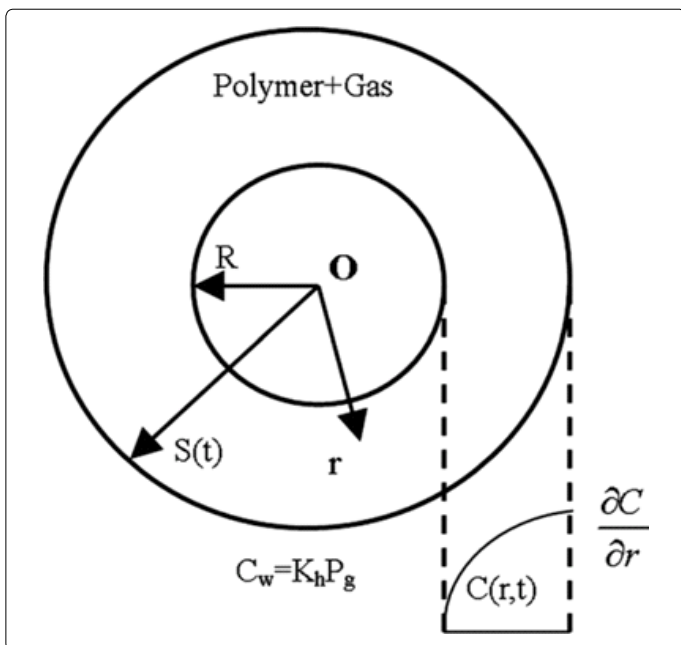


Figure 2. Schematic of the bubble growth cell model

Bubble expansion can be caused by either of the two following mechanisms [14]:

1. Hydro dynamically controlled growth
2. Diffusion-controlled growth

These two control cell growth mechanisms can be combined to yield the following differential equations [14]:

$$\left. \begin{aligned} 4\eta \dot{R} / R &= (P_g - P) - 2\gamma / R \\ \frac{d}{dt} \left(\frac{P_g R^3}{R_g T} \right) &= \frac{6\rho^2 D k_h R_g T (P_{g0} - P_g)^2 R^4}{P_g R^3 - P_{g0} R_0^3} \end{aligned} \right\} \quad (6)$$

Where η is the melt viscosity, \dot{R} is the rate of change of the radius, k_h is the Henry's law constant(solubility), P_{g0} is the initial gas pressure inside the bubble during nucleation, and P

is the pressure of the melt at the outer boundary of the cell. The internal gas pressure (P_g) is determined by diffusion, whereas the pressure at the outer boundary of the cell (P) is determined by the macroscopic pressure equation governing the molding process; ρ is the density of the gas in the bubble, D is the diffusion coefficient of the gas in the polymer melt, and R_g is the universal gas constant ($8.31451 \text{ J mol}^{-1}\text{K}^{-1}$). Solving equations 6 yields data on bubble size and gas pressure inside bubbles.

The previous sections describe the cell nucleation and growth theory. Using the physical properties of a pure gas or pure polymer physical properties to represent the physical properties of a single-phase mixed solution would clearly be inappropriate. Therefore, other physical properties such as the diffusion coefficient and melt viscosity model were modified to improve the accuracy of the bubble nucleation and growth theory for the simulation.

Surface Roughness Model

The surface roughness model can describe the relationship between the final bubble size and surface roughness [15, 16]. According to the hypothesis that the maximum surface roughness is formed when surface bubbles expand to their largest extent and burst, two simplified mathematical models of roughness can be formulated are listed in Table 1.

Table 1. Surface roughness model

Type	Symbol	Method	Scheme
Maximum roughness	R_y	Selecting the datum length "l" from crude curve alone average line direction. Absolute value of peak height and depth in this section is the R_y	
Arithmetic average roughness	R_a	Selecting the datum length "l" from crude curve alone average line direction. If the crude curve is represented by the function $y=f(x)$, R_a can be obtained by the Equation: $R_a = \frac{1}{l} \int_0^l f(x) dx$	

Height difference between the adjacent surface of the highest peak and the lowest valley is attributed to a complete breakdown caused by the bursting of an entire bubble. After the bubble bursts, the angle became passivation. The crest portion and trough portion eventually formed a both half of a cell size. Figure 3 shows a sketch of surface roughness.

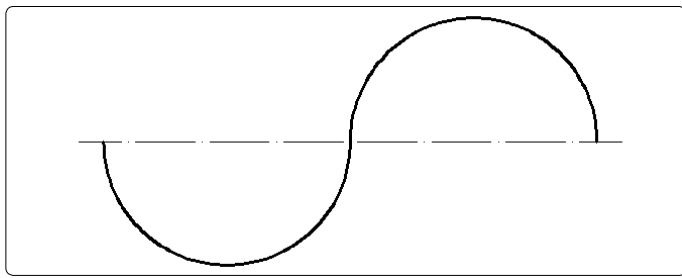


Figure 3. Surface roughness sketch

Thus, the maximum roughness R_y and the arithmetic average roughness R_a can be calculated as follows:

Maximum roughness: $R_y=2R$ (7)

Arithmetic average roughness: $R_a=\pi R^2/4R=\pi R/4$ (8)

Where R is the bubble radius nearby the melt surface, which can be calculated by the former nucleation theory and bubble growth theory. In this study, the arithmetic average roughness was used to calculate the surface roughness.

Experimental Section

Materials

Moldings were prepared using a PC/ N_2 foaming system. The properties of PC and N_2 are listed in Table 2 and 3.

Table 2. Properties of PC

Relative molecular mass	Density g/cm ³	Interfacial energy (Dynes/cm)	Bulk modulus N/cm ²	Volume expansion coefficient cm ³ /mol·K
200000	1.20	34.0	8.16×10^7	0.0575

Table 3. Properties of N_2

Density g/L	Gas constant J/(mol·K)	Molar volume V_g L/mol	Solubility cm ³ (STP)/(g·atm)
1.25	8.3145	22.4	0.032×10^{-2}

Experimental Model

A rectangular plate mold with dimensions of 100 mm (length) × 100 mm (width) × 2 mm (thickness) was designed and constructed according to the procedures of Chen et al. [17] and the applied apparatus is shown in Figure 4. Nine reference points were set for measurement of the average surface bubble data. Using a fan gate for this flat model can lower its internal stress, reduce the possibility of air involvement, and effectively eliminate any defects near the gate.

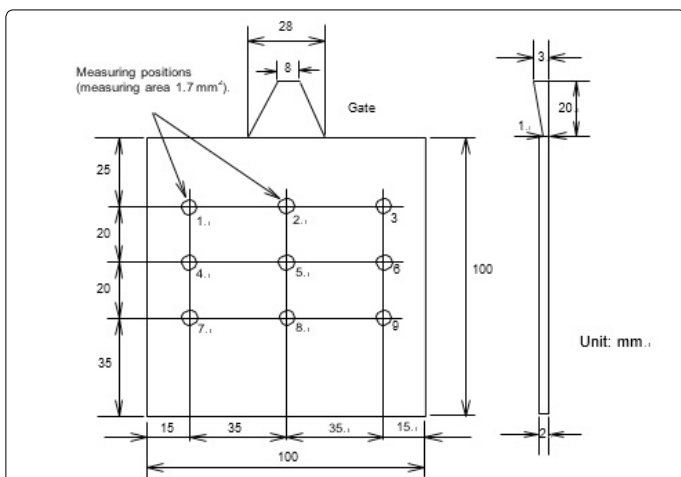


Figure 4. Schematic of the plate mold [17]

Numerical Investigations

According to the microcellular foam nucleation theory, the nucleation process parameters that must be considered including: saturation pressure, melt temperature, gas concentration, and pressure relief time. These parameters were set, and bubble quantities under different conditions are listed in Table 4. For numerical simulation, on the basis of the single phase viscosity characteristics, appropriate amendments were made to the rheological curves of PC as shown in Figure 5.

Table 4. Properties of microcellular injection nucleation

Saturation pressure/MPa	Gas concentration /cm ³	Bubble density/mol	Temperature/K	Frequency factor f_0 /(/s)	Unloading time/s	Boltzmann constant /J/K
4.14	3.70×10^{17}	1.05×10^9	383	1×10^{-5}	30	1.38×10^{-23}
6.89	6.16×10^{17}	5.34×10^9	383	1×10^{-5}	30	1.38×10^{-23}
10.34	9.24×10^{17}	1.49×10^{10}	383	1×10^{-5}	30	1.38×10^{-23}
13.79	1.23×10^{18}	9.88×10^{10}	383	1×10^{-5}	30	1.38×10^{-23}

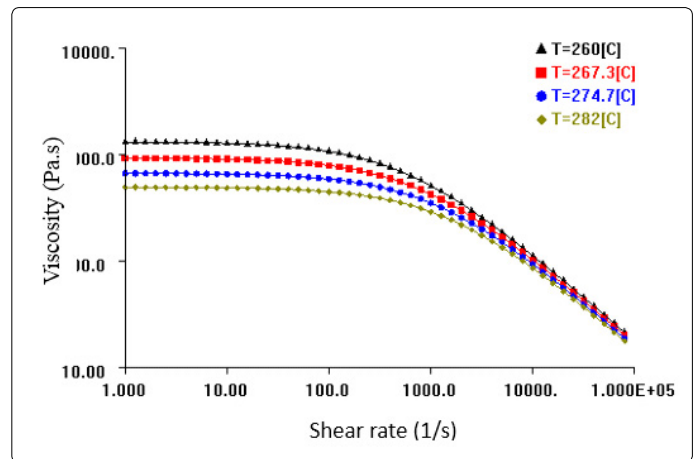


Figure 5. Rheological curves

The filling process was simulated by MOLDFLOW and the numerical analysis model was established as Figure 6. On the principle of that the mesh side length must be one times thickness of the product model, the side length was set to 2mm with a chord height of 0.1mm. Moreover, IGES tolerance was set to 0.1 mm to control mesh quality.

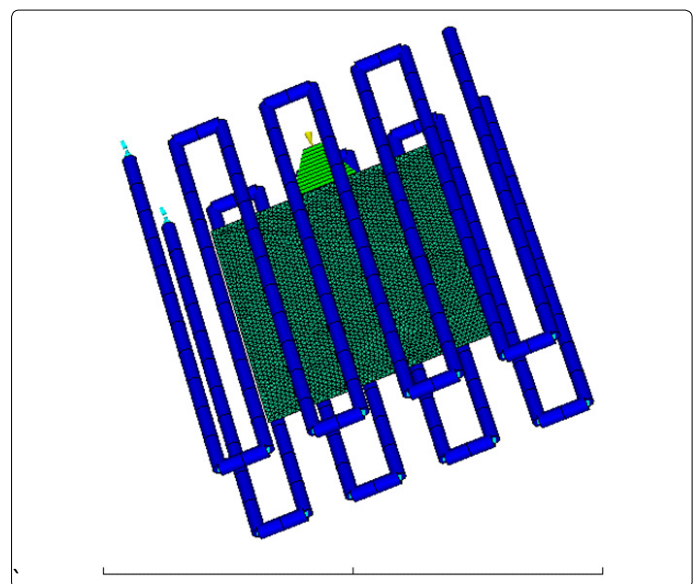


Figure 6. MOLDFLOW analysis model

The foregoing analysis of surface roughness indicated that process parameters affecting surface quality include: mold temperature, melt temperature, SCF prefill volume, injection time, and injection pressure. Herein the five parameters were studied to investigate their effect on microcellular foam injection molding. Experimental processing parameters were set as shown in Table 5.

Table 5. Microcellular injection processing parameters

parameters	values
mold temperature /°C	82
melt temperature /°C	282
SCF prefill volume /%	0.3
injection time /s	0.3
injection pressure /MPa	7.014
injection flow rate(cm ³ /s)	90

Experimental Investigations

Experimental data obtained by S.C, Chen et al. with a PC/ N₂ system were used to demonstrate the accuracy of this research. The PC resin was dried at 120°C for 3 h before processing. And the dissolving N₂ level was set at 0.3 wt% and the volume expansion ratio was set at 5% [17]. The experiment equipment and main processing parameters are listed in Table 6.

Table 6. Experimental equipment and parameters

	Property
Injection machine	Arburg 420C Allrounder 1000-350
Measuring instrument	A 3D color laser microscope (VK850, KEYENCE Corp., Japan).
Resin material	PC (HF-1130)
Supercritical fluid	N ₂ (the dissolving N2 level for 0.3%)
Volume expansion ratio	5%

When the physical processing parameters were set as the corresponding parameters had been set in the simulation, the average surface roughness of the nine positions was measured to be 26 μm, and visual inspection revealed notable flow marks on the surface, as shown in Figure 7 [17].



Figure 7. Surface of a part molded at mold temperature 60°C

Results and Discussion

Numerical Calculations of Foaming Process

The foaming process started when the melt was injected into the cavity, and lasted throughout the injection process. Considering that the pressure relief was at a steady velocity, the unloading time was counted from when melt was emitted from the gate to when the melt was cooled to its glass transition temperature, resulting in a constant $t=30$ s. According to the mentioned modified microcellular foam nucleation theory, the bubble density and critical bubble size in the foaming process can be obtained by calculating differential equations under different conditions as shown in Table 7.

Table 7. Bubble density and critical bubble size

Saturation pressure /MPa	Bubble density /cm ³	Critical bubble size/m
3.502	4.679×10^{10}	2.4×10^{-8}
7.014	9.403×10^{10}	1.18×10^{-9}
10.226	1.371×10^{11}	8.04×10^{-9}
13.806	1.851×10^{11}	5.39×10^{-9}

When the saturation pressure changed from 3.502MPa to 13.806MPa, the bubble density correspondingly changed from 4.679×10^{10} /cm³ to 1.851×10^{11} /cm³. Compared with the classical nucleation theory of microcellular foaming, nucleation as described by the modified theory was more reasonable and smoother in terms of quantity change.

Filling process

According to the previous nucleation data, when the injection pressure was 7.014MPa, the critical nucleation bubble size was 1.18×10^{-9} m. When the initial foam volume ratio was 95%, the bubble density was 9.403×10^{10} /cm³. These data were set as boundary conditions in MOLDFLOW. The filling process was then simulated and the surface injection time and melt temperature were obtained. The simulation results of the fifth reference point were as shown in Figure 8 and 9.

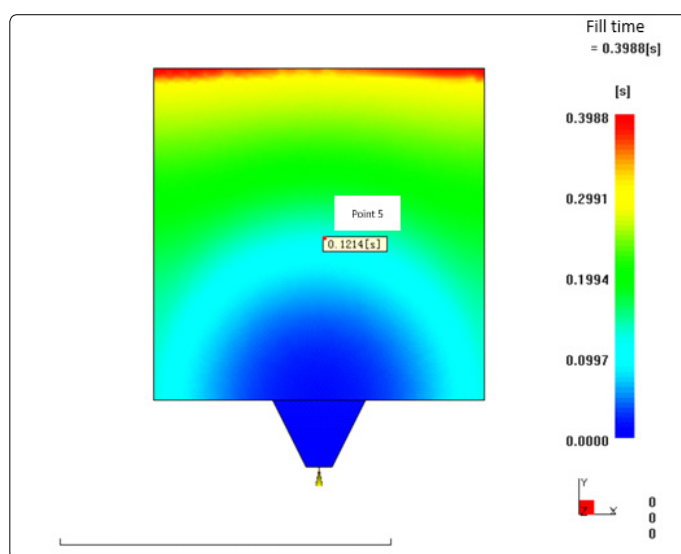


Figure 8. Fill time of the fifth point

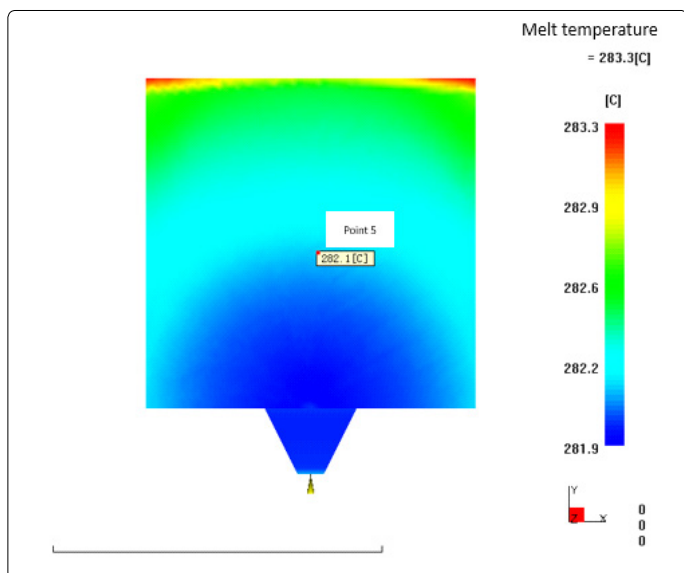


Figure 9. Temperature at the flow front of the fifth point

The injection time of melt flowing to the fifth reference point was $t = 0.1214$ s, and the melt temperature at the flow front was $T = 282.1^\circ\text{C}$. The results for all reference points' results were shown in Table 8.

Table 8. Fill times and temperatures of flow front at nine reference points

Point number	1	2	3	4	5
Injection time (s)	0.0873	0.0542	0.0867	0.1535	0.1214
Melt temperature (°C)	282.2	282.2	282.2	282.1	282.1
Point number	6	7	8	9	
Injection time (s)	0.1550	0.2390	0.2326	0.2396	
Melt temperature (°C)	282.1	282.0	282.0	282.0	

Bubbles' Growth Profiles and Calculation of Surface Roughness

This part was thin-walled, and as shown in Table 8, the temperature difference were negligible, therefore the melt temperature during the filling process can be considered constant until the melt fills the whole model. Thus, the viscosity of the melt can also be considered to be constant. At a definite shear rate, the viscosity of the pure melt along with the change of temperature can be expressed by the Arrhenius Equation. Subsequently, through the modification of the viscosity equation, the formula of melt viscosity under a shear rate of 100/s was obtained as follows:

$$\eta = 1.6505 \times 10^{-7} \times e^{\frac{1.002e5}{RT}}$$

The flow front temperature of the fifth reference point is 282.1°C . Through substitution into eq. 9, the viscosity of the melt can be calculated as $\eta = 440.74$ Pa·s. The boundary conditions at bubble growth of the fifth reference point are listed in Table 9.

Table 9. Boundary conditions of calculation for surface bubble radius at the fifth reference point

Fill time/s	Critical bubble size/m	Injection pressure/MPa	Molding temperature/°C	Gas diffusion coefficient D	Viscosity/Pa·s
0.1214 4	1.2e-9	7.014	282.1	2.4258e-9	440.74

Through the use of Runge-Kutta single-step programming algorithm in MATLAB, bubble profile data can be obtained by

solving the ordinary differential equations of eq.1 and eq.6. The surface bubble size of the fifth reference point was calculated as $27.20 \mu\text{m}$. The relationship of bubble radius versus time is shown in Figure 10 and the relationship of pressure inside the bubble versus time is shown in Figure 11.

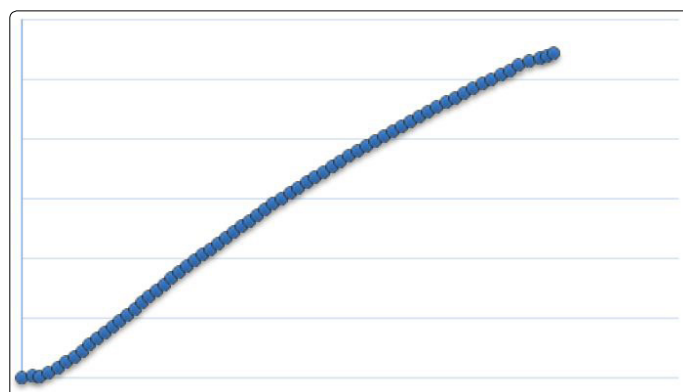


Figure 10. Bubble radius versus time (t/s) during the fill time at fifth reference point

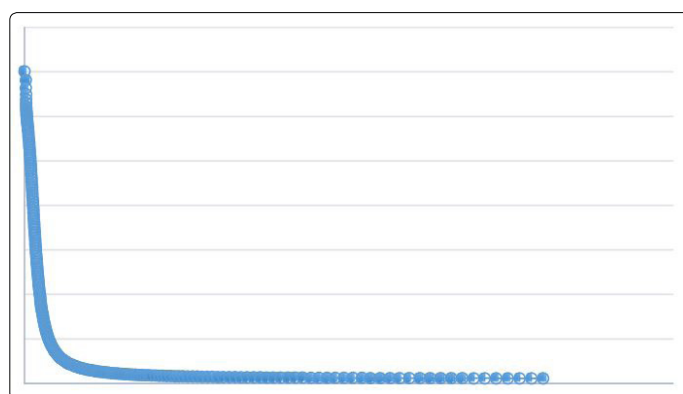


Figure 11. Pressure inside the bubble versus time during the fill time at fifth reference point

As shown in Figure 10 and 11, the pressure inside the bubble dropped rapidly and the bubble radius grew slowly. This conformed to the rule that pressure transmission in polymer is in the form of mechanical waves. Thus, the pressure inside the bubble rapidly reached equilibrium with the pressure outside. The nucleation process can be considered mainly complete at the pressure relief stage, thus, as the pressure stabilized, the main driving force of bubble growth was the SCF concentration gradient between the solution and the bubble. The surface bubble size for all the nine reference points were obtained (Table 10) through the same analysis methods as in previous calculation.

Table 10. Bubble radii at reference points

Point number	1	2	3	4	5
Bubble size (μm)	20.05	12.68	19.93	31.47	27.20
Point number	6	7	8	9	
Bubble size (μm)	31.69	42.73	41.97	42.80	

As presented in Table 10, three points of each set conformed to a progressive increase in bubble size, and differences in bubble size between the nine points were not large, Thus confirming that the farther the bubble was from the gate, the larger the bubble size was. The average bubble size for all nine reference points in the model was $R = 30.06 \mu\text{m}$. According to the mentioned surface roughness model,

the arithmetic average roughness was calculated by

$$Ra = \frac{1}{l} \int_0^l f(x) dx = \pi R^2 / 4R = \pi R / 4 = 23.61 \mu m$$

The average surface roughness calculated by numerical analysis, namely Ra = 23.61 μm was closely approximated the experimental result of Ra = 26 μm. The numerically simulated roughness results for all points were close to the experimental volatility results. This approximate equality shows that this investigation could depict the surface roughness behaviors with considerable accuracy.

Range Analysis and Variance Analysis of Orthogonal Experimental Method

According to the orthogonal experimental method, surface roughness was considered as an objective function, of which the influencing factors were the melt temperature, mold temperature, SCF content, melt pressure, and injection time. Because of the difficulty of achieving a high mold temperature condition in actual production, the mold temperature was set to a low temperature range. The levels of these five parameters were set as shown in Table 11.

Table 11. Process parameters list

Parameters	1	2	3	4
Melt temperature°C	262	268	274	280
Mold temperature°C	60	66	72	78
SCF content (%)	0.1	0.3	0.5	0.7
Melt pressure (MPa)	3.502	7.014	10.226	13.806
Injection time (S)	0.15	0.2	0.25	0.3

An L₁₆ (4⁵) orthogonal array was applied for this orthogonal analysis. A total of 16 groups of tests were conducted. The average surface roughness values of all test groups, obtained by numerical calculation, are shown in Figure 12.

Figure 12. Average surface roughness values of all test groups

Results derived from analysis of the range R and variance S of single factors are shown in tables 12 and 13 respectively.

Table 12. Results of range analysis and variance analysis of each process parameter

	Melt temperature	Mold temperature	SCF content	Melt pressure	Injection time
l ₁	20.25	25.21	25.45	7.83	17.05
l ₂	24.1	22.23	22.81	18.9	22.05
l ₃	23.35	22.82	22.08	28.22	25.53
l ₄	24.19	22.11	22.02	37.42	27.74
R _i	3.94	3.09	3.43	29.59	10.69

Table 13. Variance analysis of each process parameter

	Melt temperature	Mold temperature	SCF content	Melt pressure	Injection time
S _{sf}	10.36	6.27	7.81	482.09	65.14
F _i	0.00455	0.00275	0.00343	0.21172	0.02861
C _i	1.81%	1.10%	1.37%	84.33%	11.39%

where F_i is the degree of influence of each parameter on the experimental results, C_i is the contribution ratio of each parameter.

As presented in tables 12 and 13, the process parameters that exerted the greatest effect on the roughness (in descending order) were melt pressure, injection time, melt

temperature, SCF content, and mold temperature. These results were consistent with the intuitive analysis:

1. The melt viscosity decreased as the melt temperature rose, thus, the bubble growth resistance force decreased and the final bubble size increased.
2. The decline in SCF content resulted in a concentration difference and a decline in the driving force of bubble growth, therefore, the final bubble size decreased.
3. As the melt pressure decreased, the cavity pressure decreased, hence, the final bubble size decreased.
4. As the injection time decreased, the bubble growth time decreased, therefore, the final bubble size decreased.
5. When the mold temperature was set in a low temperature range, the effect of mold temperature on surface roughness was not obvious.

Conclusion

This study demonstrated bubble nucleation and growth processes in microcellular foam injection part, and part surface roughness values were calculated by a numerical scheme. On the basis of nucleation theory and bubble growth theory, nucleation density, and critical bubble size of bubble nucleation as well as the subsequent bubbles' growth profiles were given. According to the surface roughness calculation model, the average surface roughness value was calculated as R_a= 23.61um, which was comparable to the experimental value of R_a = 26um .This close fit indicates that the proposed method could characterize and predict surface roughness formation and that the proposed method can guide further research regarding surface bubble burst mechanisms. This study provides a complete theoretical model of surface roughness in microcellular foam injection molding, and the effect of process parameters on surface roughness were analyzed.

Acknowledgement

The authors thank Shanghai Nature Foundation, China (No.13ZR1420500) for financial support.

References

1. Martini J, Waldman F, Suh N. The production and analysis of microcellular thermoplastic foam. *SPE ANTEC Technical Papers*. 1982; 28: 674-76.
2. Martini J, Suh NP, Waldman FA. Saturation with inert gas, depressurization, and quick-cooling, in, Google Patents, 1984.
3. Hu GH. Reasearch on key technologies of microcellular foam injection moulding process [D] in Shanghai: Shanghai Jiao Tong University, 2009.
4. Wang GL, Zhao GQ, Wang JC, Zhang L. Research on formation mechanisms and control of external and inner bubble morphology in microcellular injection molding. *Poly Eng & Sci*. 2015; 55(4): 807-835. doi: 10.1002/pen.23948
5. Chen HL, Chien RD, Chen SC. Using thermally insulated polymer film for mold temperature control to improve surface quality of microcellular injection molded parts. *Int Commun in Heat and Mass Tran*. 2008; 35(8): 991-94. doi: 10.1016/j.icheatmasstransfer.2008.04.017

6. Cha SW, Yoon JD. The relationship of mold temperatures and swirl marks on the surface of microcellular plastics. *Polymer-Plastics Technology and Engineering*. 2005; 44(5): 795-803. doi: 10.1081/PTE-200060811
7. Michaeli W, Cramer A. Increasing the surface quality of foamed injection molded parts, in: Proceedings of the 64th Annual Technical Conference (ANTEC) of the Society of Plastics Engineers, Charlotte, Vereinigte Staaten von Amerika, 2006.
8. Colton JS, Suh NP. Nucleation of microcellular foam: theory and practice. *Poly Eng & Sci*. 1997; 27(7): 500-503. doi: 10.1002/pen.760270704
9. Hu GH, Jiang CD, Cui ZS. Relationship between Microcellular Foaming Injection Molding Process Parameters and Cell Size. *Journal of Donghua University*. 2008.
10. Zhao DX, Hu GH, Wang ZY. Cell Nucleation Theory of Microcellular Foam Injection Molding. *Plastic*. 2009.
11. Li H, Leung SN, Park CB, Li G. The consequences of approximating the classical nucleation theory in simulation of polymer foaming process. *SPE ANTEC Technology Papers*. 2005.
12. Kim KY, Kang SL, Kwak HY. Bubble nucleation and growth in polymer solutions. *Poly Eng & Sci*. 2004; 44(10): 1890-899. doi: 10.1002/pen.20191
13. Amon M, Denson CD. A study of the dynamics of foam growth: analysis of the growth of closely spaced spherical bubbles. *Poly Eng & Sci*. 1984; 24(13): 1026-1034. doi: 10.1002/pen.760241306
14. Han S, Kennedy P, Zheng X, Kishbaugh L. Numerical analysis of microcellular injection molding. *Journal of cellular plastics*. 2003; 39(6): 475-85. doi: 10.1177/0021955X03039214
15. Liu L, Loh NH, Tay BY, Tor SB, Murakoshi Y, Maeda R. Effects of thermal debinding on surface roughness in micro powder injection molding. *MaterLetts*. 2007; 61: 809-12. doi: 10.1016/j.matlet.2006.05.070
16. Erzurumlu T, Oktem H. Comparison of response surface model with neural network in determining the surface quality of moulded parts. *Materials & Design*. 2007; 28(2): 459-465. doi: 10.1016/j.matdes.2005.09.004
17. Chen SC, Lin YW, Chien RD, Li HM. Variable mold temperature to improve surface quality of microcellular injection molded parts using induction heating technology. *Advances in Polymer Technology*. 2008; 27(4): 224-32. doi: 10.1002/adv.20133